LOAD DISTRIBUTION IN ROLLING FRICTION GUIDEWAYS

H.R. El Sayed, T. Elwardany and E.A. Soliman
Production Engineering Department, Faculty of Engineering,
Alexandria University, Alexandria, Egypt.

ABSTRACT

Rolling friction guideways have proven themselves in numerous applications. They provide economical solutions for most guidance problems and are widely used in constructing feed and motion heads of machine tools. However, the designer of such type of guideways is usually confronted with the problem of selecting the proper configuration, which depends to a large extent upon the load distribution on the different rolling elements. A general equation specifying the load distribution in the different configurations of rolling friction guideways will thus provide the necessary solution for the problem of selecting and designing these guideways. For these reasons, this work will be devoted to establishing such solution.

INTRODUCTION

Rolling friction guideways [Abr.R.F.Gs] are those guideways in which intermediate rolling members, balls or rollers are inserted between the guideway surfaces.

A R.F.G. is composed of a stationary part, a moving part, rolling elements and a cage, Figure (1). R.F.Gs are manufactured to possess several configurations, the common ones are the V-V Ball, F-V Ball, V-V Roller and F-F Roller and are shown in Figure (2).

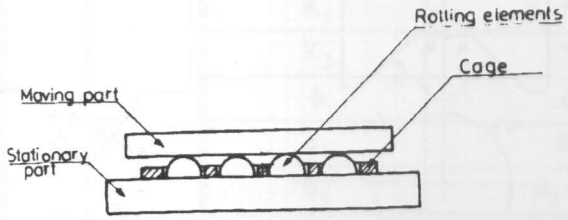

Figure 1. Elements of a rolling friction guideway.

The load carried by any R.F.G is distributed on its rolling elements. This distribution represents the major factor affecting the R.F.G. performance. For this reason, several authors tried to predict expressions for the load distribution on R.F.Gs. J. Housa [1] assumed a linear relation between the loads acting on the rolling elements and their deformations. This assumption destroys the accuracy of the analysis even within the elastic limits. S. Chigeo and I. Minoru [2,3] calculated the load distribution on a group of rollers engaged between two flat plates. In their experimental work, the used test rig did not simulate the actual guideway.

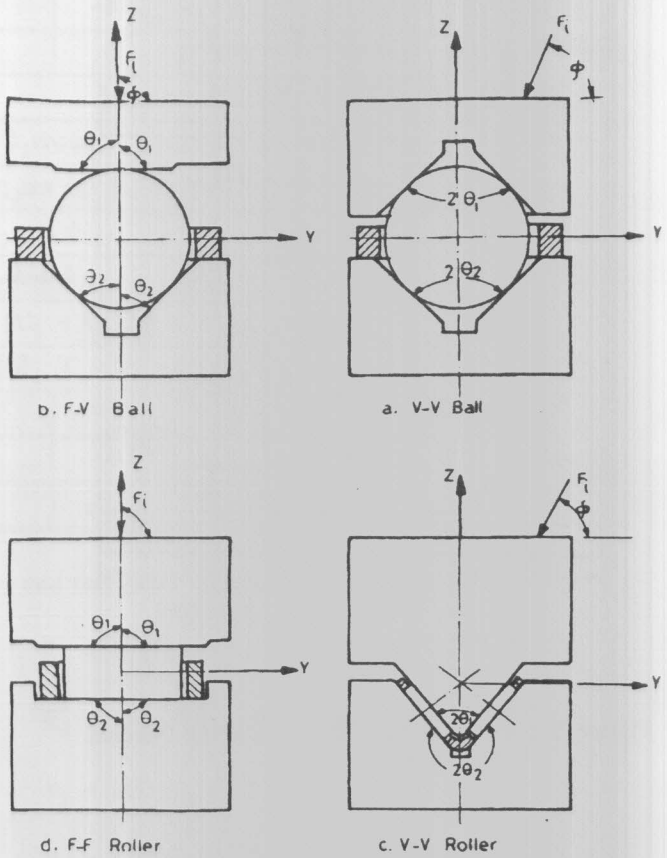

Figure 2. Configurations of guideways elements.

The rollers were in contact and the two plates were fixed. Z.M. Levina [4] studied the effect of the geometrical error of the moving part on the load distribution on rolling elements between two flat plates. He assumed the reaction

properties of fuel. Parks et al. [4] investigated the effect of gas temperature on both gas viscosity and evaporation rate to establish a correlation for the penetration of diesel fuel sprays in gases. The spray penetration was correlated by an equation based on the standard density of atmospheric air, a reference orifice diameter, gas temperature and the pressure drop across nozzle orifice. Burt and Troth [5] proposed a correlation for spray penetration in terms of gas density, time and an empirical constant. The tests were conducted inside a cold bomb, using single injection of gasoline, kerosene and heavy gas oil into nitrogen. Taylor and Walsham [6] conducted cold-bomb tests using single gas oil injection into nitrogen. Conventional and schlieren visualization techniques were used to track the spray. Williams [7] developed a theoretical model to calculate the penetration results for diesel fuel sprays. The model is based on the theory of the homogeneous, constant-momentum, steady jet. The resulting equation for momentum rate involves jet density, centerline velocity and the distance from nozzle tip to a point on the jet axis. Williams used the results of Schweitzer [1], Joachim [24], Burt and Troth [5], Pischinger [25] and Parks et al. [4] in order to determine the equation constant. Hiroyasu et al. [8] used a constant-volume bomb to study spray penetration. Injection pressures were 7,10 and 15 MPa. The chamber was supplied with nitrogen at pressures of 1,2 and 3 MPa. Chamber temperatures were 22, 150 and 320° C. Henein and Fragoulis [9] developed an empirical correlation for calculating spray penetration in which the concept of "mean penetration diameter" was introduced. The approach assumed a single droplet undergoing insignificant evaporation during its trajectory, and the jet was assumed to be steady. Koo and Martin [10] experimentally obtained a relation between droplet sizes and velocities for transient diesel fuel spray. The approach used a quiescent chamber at atmospheric temperature and pressure. Arold et al. [11] constructed a DI diesel engine for the optical investigation of in-cylinder flow fields, spray combustion and emissions phenomena. Single laser doppler velocimetry (LDV) and high speed movies recorded the flow conditions for both square and round combustion chambers. Singh and Henein [12] developed a mathematical model for the penetration of a transient fuel spray in a direct injection diesel engine. Mass and momentum conservation equations were used to compute the penetration of fuel spray. They assumed that the spray was divided into ten concentric spray cones. The calculated distances of penetration were compared with experimental data, and reasonable agreement was obtained. Kiichiro et al. [13] developed an empirical correlation for the droplet size distribution as a function of time and displacement. They used microscopic photography and studied varying back pressure and ambient density.

El-kotb [14] described a numerical procedure capable of predicting the local flow pattern in combustors. The model solved the Eulerian equation of gas phase and the Lagrangian equations of the droplet motion. The statistical spray model used by Westbrook [26], Cliffe [27], and Bracco et al. [28] considered a general spray distribution function originally defined in space by droplet diameter, location, velocity and time.

Droplet vaporization models have been classified into two major categories : Spherical-symmetry models and axisymmetric models [15]. One of the spherical-symmetry models is the famous d^2-law model which assumes a linear relationship between the droplet surface area and time [16]. Henein [17] applied the same model to iso-octane and found the results to be in good agreement with Faeth's experiments [18]. The second of the spherical-symmetry models is the conduction limit model. This model neglects the internal circulation within the droplets, and results in non-uniform temperature distribution. Lakshminarayan and Dent [19] studied the concentration and temperature distribution in transient vapourising non-burning and burning fuel sprays. Empirical relations obtained the axial and radial variations of concentration in the vapourising fuel. Prakash and Sirignano [20] developed a two-dimensional axisymmetric model in order to study the cases in which the Reynolds number is very large compared to unity. Tong and Sirignano [21] simplified the axisymmetric model, and found the accuracy of the results still acceptable. Van Gerpen et al. [22] studied the effect of air swirl, injection pressure and nozzle geometry on exhaust particulates, Nitrogen Oxides emissions, ignition delay, heat release and local heat flux measured at two positions on head of a single cylinder open chamber diesel engine of the TACOM-LBECO type. Megahed et al. [23] developed a computer model to calculate the transport properties of a single droplet during vaporization in heterogeneous combustion systems. A fourth-order Runge-Kutta technique was used to determine the liquid phase properties and the film properties in terms of time. However, the model was developed for droplets suspended statically in hot environment. The cases of droplet motion were not covered by the model.

The aforementioned review reveals that many research works were conducted on spray behavior in conventional

diesel engines. As for adiabatic diesel engines, most of the research activities were directed towards hardware development (engine components and systems). Fundamental investigations of combustion characteristics in adiabatic engines are still in the phase of exploring the various stages of spray development and evaporation. Therefore, the aim of the present work is to introduce a model for the penetration and evaporation of fuel droplets subjected to excessively high temperatures. The model takes into consideration the variations of the physical properties due to the high temperatures in the adiabatic diesel engine as well as the droplet velocity and the resulting influence on the rate of heat transfer and the evaporated mass of the droplet.

ANALYSIS

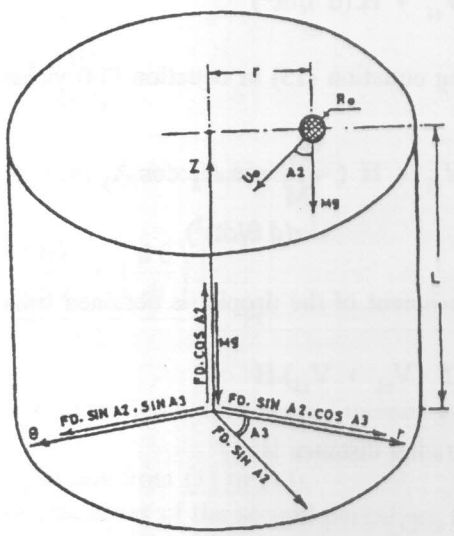

Figure 1. Analysis of Forces acting on a fuel drop.

Figure (1) illustrates the forces acting on a fuel droplet injected through a gaseous environment of temperature T_G. The droplet has an initial injection velocity U_0. The following assumptions are made:

1. The individual droplet is assumed to have the spherical shape.
2. The individual droplet is treated as a projectile from the injector nozzle with initial velocity U_o.
3. The interaction between neighboring droplets is neglected.
4. No concentration or temperature gradients exist within the droplet.
5. The thickness of the vapour film surrounding the droplet is assumed to be of the order of magnitude of the droplet radius.
6. The arithmetic mean temperature is used for calculating the average properties of the film.
7. The gas used in the model is nitrogen.

It is well known that diesel fuel is a mixture of tens of pure hydrocarbon compounds of widely different properties. The composition of this mixture differs according to the type of the crude oil and the method of crude processing. Moreover, different batches of diesel fuel produced at the same refinery may never have the very same properties. Therefore, the mathematical modeling of the evaporation and combustion of diesel fuel would be extremely cumbersome without a reasonable approximation according to which a pure substance is selected as a representative of diesel fuel. It has been found that dodecane (C_{12} H_{26}) is the hydrocarbon in the paraffin family with properties closest to those of diesel fuel (e.g. density, enthalpy of vaporization, heating value, ignition delay characteristics, etc.). And, therefore, dodecane is the fuel used in the mathematical modeling of the present work.

The equation of motion of the fuel droplet may be written as follows :

$$F_D = C_D \cdot (0.5 \cdot \rho_a \cdot U^2) \cdot \pi \cdot R^2 \qquad (1)$$

where the drag coefficient changes according to the Reynolds number [Ref.9].

$$C_D = 24/Re \qquad \text{for } Re \le 1$$

$$C_D = 24/(Re)^{0.646} \qquad \text{for } 1 < Re \le 400$$

$$C_D = 0.5 \qquad \text{for } 400 < Re \le 3\times10^5$$

$$C_D = 0.000366\times(Re)^{0.4275} \qquad \text{for } 3\times10^5 < Re \le 2\times10^6$$

where the Reynolds number equation is defined by

$$Re = 2\ \rho_a\ U\ R/\mu_a \qquad (2)$$

The mass of the droplet M is as follows

$$M = (4/3)\ \pi\ R^3\ \rho_L \qquad (3)$$

The droplet leaves the injector nozzle with initial conditions R_o, U_o, M_o, r, L, and θ as shown in Figure (1). The equation of motion in Z-direction using Newton's second low in the Z-direction is,

$$M.a_z = M.g - F_{DZ} \qquad (4)$$

The acceleration in the Z-direction is:

$$a_Z = d^2Z/dt^2 \qquad (5)$$

The velocity equation according to Newton's second low is:

$$V_Z = \int a_z.dt + \text{constant} \qquad (6)$$

For an infinitesimal increment of time H, the acceleration a_Z may be assumed constant, and

$$V_{Z2} = V_{Z1} + a_z.H$$

The velocity in the differential form is:

$$V_Z = d_Z/dt \qquad (7)$$

The initial velocity component in the Z-direction is given by:

$$V_{Z0} = U_o \cos A_2 \qquad (8)$$

Eqs. (6),(7) and (8) yield:

$$V_Z = dZ/dt = U_o \cos A_2 + (g - \frac{F_D \cos A_2}{M}).H \qquad (9)$$

The distance of droplet from the injector nozzle towards cylinder surface in the Z-direction yields:

$$D_Z = V_{Z0}.H + 0.5\ a_Z\ H^2 \qquad (10)$$

From Figure (1), the analysis of forces acting on droplet in r-direction yields:

$$Ma_r = -F_{Dr} \qquad (11)$$

The force F_{Dr} is related to the resultant F_D by:

$$F_{Dr} = F_D \sin A_2 \cos A_3 \qquad (12)$$

And therefore:

$$a_r = -\frac{F_D}{M} \sin A_2 \cos A_3 \qquad (13)$$

The velocity V_{r2} after a time increment H is given by

$$V_{r2} = V_{r1} + H.(d^2r/dt^2) \qquad (14)$$

Substituting equation (13) in equation (14) yields :

$$V_{r2} = V_{r1} + H\ (-\frac{F_D}{M} \sin A_2 \cos A_3 + r(d\theta/dt)^2)$$

The displacement of the droplet is obtained from,

$$D_r = 0.5\ (V_{r1} + V_{r2}).H$$

while the radial distance is :

$$r_2 = r_1 + D_r$$

Using Newton's second law in the θ-direction, Figure yields :

$$M.a_e = -F_{D\theta}$$

The force in direction yields :

$$F_{D\theta} = F_D \sin A_2 \sin A_3$$

Dividing equation (17) by M and substituting for thence

$$a_\theta = -(F_D/M) \sin A_2.\sin A_3$$

Since the acceleration in θ-direction is :

$$a_\theta = r\left[d^2\theta/dt^2\right] + 2[dr/dt]\,[d\theta/dt] \tag{19}$$

Therefore,

$$d^2\theta/dt^2 = [a_\theta - 2(dr/dt)(d\theta/dt)]/r \tag{20}$$

For the first infinitesimal increment of time (H) the differential equation for the velocity in the θ-direction is:

$$\left(\frac{d\theta}{dt}\right)_2 = \left(\frac{d\theta}{dt}\right)_1 + \left(\frac{d^2\theta}{dt^2}\right)_1 . H \tag{21}$$

and the velocity $V_{\theta 2}$ is determined by :

$$V_{\theta 2} = r_2\left(\frac{d\theta}{dt}\right)_2 \tag{22}$$

The displacement D_θ is calculated by :

$$D_\theta = \frac{\left[\left(\frac{d\theta}{dt}\right)_1 + \left(\frac{d\theta}{dt}\right)_2\right]}{2} . H \tag{23}$$

The equations of motion for the second increment of time H are
the same equations from (1) to (23).

The initial conditions of the second period are the final conditions of the first period.

The magnitude of the velocity of the second increment is given by

$$U_1 = \sqrt{|V_z|^2 + |V_r|^2 + |V_\theta|^2} \tag{24}$$

Also the velocity vector direction is calculated from :

$$A_2 = \cos^{-1}\left(\frac{V_z}{U_1}\right) \quad \text{and} \quad A_3 = \sin^{-1}\left(\frac{V_{\theta 2}}{U_1}\right)$$

$$s = \sqrt{(x_2-x_1)^2 + (y_2-y_1)^2 + (z_2-z_1)^2} \tag{25}$$

where (x_1, y_1, z_1) and (x_2, y_2, z_2) are initial and final cartesian coordinates, respectively.

Mass Conservation of the Fuel Droplet:

The rate of decrease in liquid droplet mass is equal to the rate of increase of mass surrounding vapour film; i.e.

$$\frac{dm_L}{dt} + \frac{dm_V}{dt} = 0 \tag{26}$$

where:

$$\frac{dm_L}{dt} = \frac{d}{dt}\left(\frac{4}{3}\,\pi\,\rho_L\,R^3\right) \tag{27}$$

Upon the study of orders of magnitudes, it is indicated that

$$R^3\left(\frac{d\rho_L}{dt}\right) < 3\,R^2\,\rho_L\left(\frac{dR}{dt}\right)$$

then equation (27) may be rewritten as :

$$\frac{dm_L}{dt} = 4\,\pi\,\rho_L\,R^2\left(\frac{dR}{dt}\right) \tag{28}$$

Energy Conservation of the Fuel Droplet:

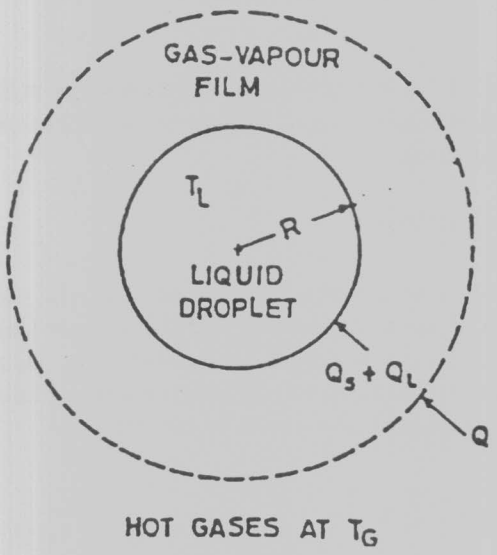

Figure 2. Liquid droplet and surroundings.

Figure (2) shows that the heat flow rate absorbed through the droplet surface is equal to the rate of change of internal energy plus the rate of energy used for evaporating an incremental volume of the liquid phase. The radiative terms are neglected in the absence of flames because of their small value, i.e.

$$4\pi R^2\bar{h}(T_G - T_L) = \frac{4}{3}\pi R^3 \rho_L C_L \frac{dT_L}{dt} - 4\pi R^2 \rho_L h_{fg} \frac{dR}{dt} \quad (29)$$

Equation (29) is true as long as :

$$R(dX/dt) < X\,(dR/dt)$$

where X is any liquid-phase property (ρ_L, C_L, T_L or h_{fg}). The mean heat transfer coefficient $\bar{h}$ is given by Ranz and Marshall [42] as :

$$\overline{Nu} = \frac{\bar{h}(2R)}{\bar{k}} = 2 + 0.6\, Re^{1/2}\, Pr^{1/3} \quad (30)$$

Substituting equation (30) in (29) gives:

$$\frac{dR}{dt} = \frac{1}{3} R \frac{C_L}{h_{fg}} \frac{dT_L}{dt} - \frac{\bar{k}(1 + 0.3\, Re^{1/2} Pr^{1/3})}{R \rho_L h_{fg}} (T_G - T_L) \quad (31)$$

Equation (31) is the differential equation to be solved to give the change of the liquid droplet radius with respect to evaporation time.

Solution Technique:

Assuming constant-pressure surroundings, the physical properties of both the droplet and the surrounding film depend mainly on the liquid temperature. The history of the droplet temperature may be described by the following equation which was introduced by Henein [17].

$$T_L = T_{eq} - (T_{eq} - T_{Lo})\, e^{-\beta t} \quad (32)$$

The equilibrium temperature T_{eq} is defined as the temperature of the liquid at which all the energy reaching the droplet surface is used for evaporating the liqui phase. In other words, it is the temperature at whic $dT_L/dt = 0$. For atmospheric pressure T_{eq} will correspon to the normal boiling point of the liquid fuel.

Since the properties $\bar{k}$, ρ_L, h_{fg} and C_L in equation (3 are temperature-dependent, and since the temperature T (according to equation (32) is time-dependent, therefor the rate of change of droplet radius dR/dt of equatio (31) can be expressed in the general form by:

$$\frac{dR}{dT} = F(R,t) \quad (33)$$

which is a first-order ordinary differential equation tha can be solved numerically by using a fourth-orde Runge-Kutta technique. The constant ß in equation (32 is calculated by :

$$\beta = \left\{ \frac{3\bar{k}}{R^2 \rho_L C_L} \left(\frac{T_G - T_L}{T_{eq} - T_L} \right) + \frac{3 h_{fg}}{R C_L (T_{eq} - T_L)} \cdot \frac{dR}{dt} \right\}\Bigg|_{t=0} \quad (34)$$

Knowing the values of T_{eq} and ß the history of the liquid droplet temperature T_L can be determined from equation (32). For momentum conservation, the droplet is assumed as a homogeneous sphere of fuel, to be injected from the injector with initial conditions R_o, $\bar{U}_o$. When the droplet is released from the injector, it passes through hot gas in the cylinder. The droplet properties change with time, and this affects the motion of droplet. The Reynolds number, the coefficient of drag and the drag force are calculated. The Runge-Kutta technique determines the liquid and vapour phase properties in terms of time. The instantaneous rate of change of the droplet radius dR/dt is calculated from equation (31). This rate is used for determining the radius after an incremental time H. The equations used to calculate the physical properties of both the liquid and vapour phases in terms of the temperature are based on refs. [30-41].

A computer program was developed and run using a suitable time increment for computations. The program was then rerun using a smaller time increment (usually 50% of the first increment). The values of dM/dt and $\delta Q/dt$ for both runs were compared. When the error was less than 3%, computations were terminated. Otherwise, a smaller time increment was used, and a new history of

vaporization was calculated. The reason for selecting dM/dt and $\delta Q/dt$ to verify the accuracy of computations is that the mass rate of vaporization and the rate of heat transfer depend on the droplet size, the properties of both the liquid and vapour phases and initial velocity of droplet. Therefore, by setting the error in computing dM/dt and $\delta Q/dt$ at 3%, the computational error for the properties must be less than 3%. The end of vaporization was fixed by the time when over 98% of the initial droplets mass was evaporated.

The validity of the present model was checked by comparing it with Megahed's model [23,43] for the initial velocity U_o equal to zero. The comparison showed a close agreement. It should be pointed out that Megahed's model was based on the assumption of suspended droplets, meanwhile the dynamic behaviour of the droplet is taken into account according to the present model.

RESULTS AND DISCUSSION

The history of droplet velocity is shown in Figure (3) for three values of initial velocity U_o of 100, 200, and 400 m/s. The Figure shows that the higher the initial velocity the higher would be the deceleration due to the increase in the drag forces (Eqs. 1,4). It is pointed out here that the droplet velocity decays for $U_o = 400$ m/s faster than for $U_o = 100$ m/s due to the effect of the Reynolds number on increasing the rates of heat transfer and evaporation of the liquid phase. This would result in reducing the droplet mass at a high rate; this means a smaller droplet momentum and a shorter time of penetration.

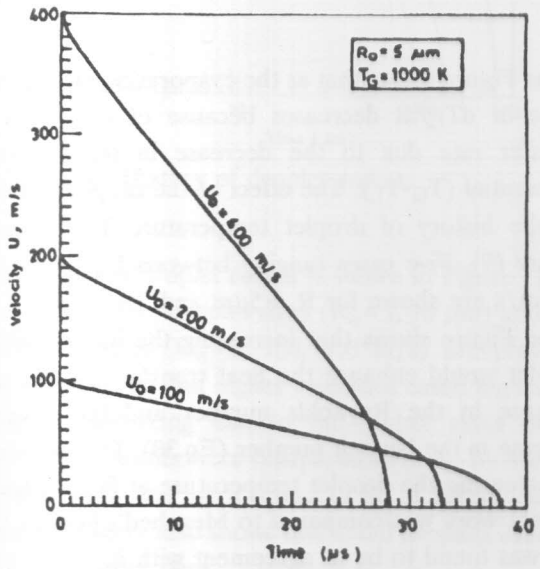

Figure 3. History of droplet velocity.

The history of droplet penetration is shown in Figures (4), (5) and (6). The effect of the initial radius R_o is shown in Figure (4) for the values of Ro = 1, 5, and 10 μm.

The Figure shows that the larger the droplet, the further would be the penetration distance S. Figure (5) shows that higher gas temperatures shorten the evaporation time and, consequently, causes the droplet to disappear before it travels a long distance. The Figure shows that the penetration distance is 1.8 mm for T_G = 1200 K and 3.2 mm for T_G = 800 K. The effect of the initial velocity U_o of the droplet on the history of penetration distance is shown in Figure (6). The Figure shows that faster droplets travel more distance than slower ones.

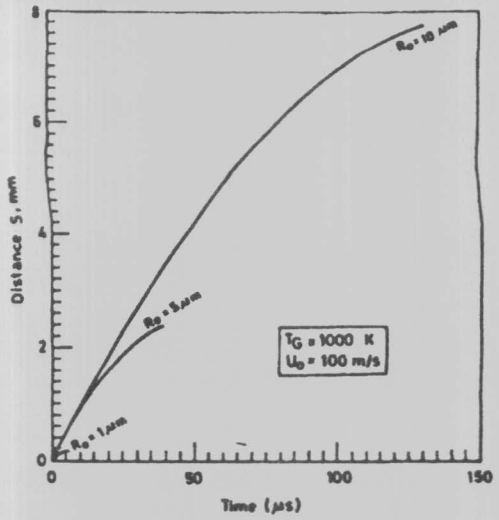

Figure 4. Effect of droplet radius R_l on the history of penetration.

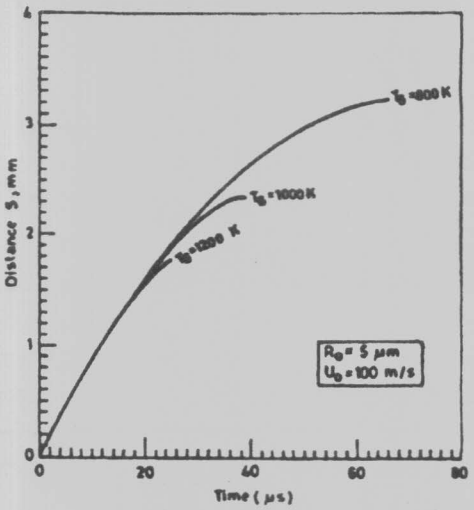

Figure 5. Effect of gas temperature T_G on the history of penetration.

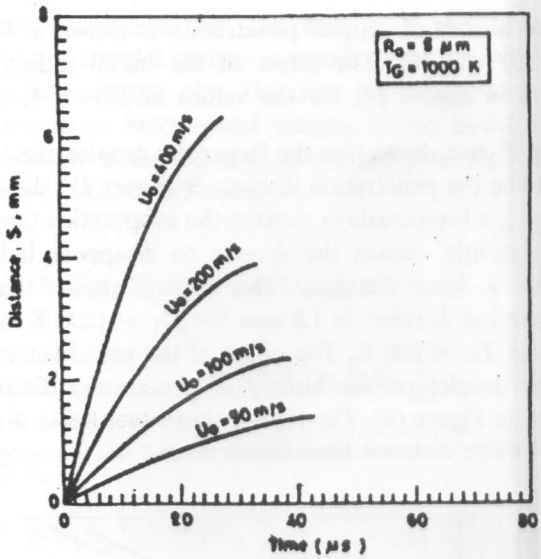

Figure 6. Effect of droplet velocity U_o on the history of penetration.

A droplet having an initial velocity U_o = 400 m/s would travel 6.3 mm in 28 μs while mother droplet having U_o = 50 m/s would travel 1.4 mm in 43 μs.

The effects of the droplet size and gas temperature on the history of droplet temperature are shown in Figure (7).

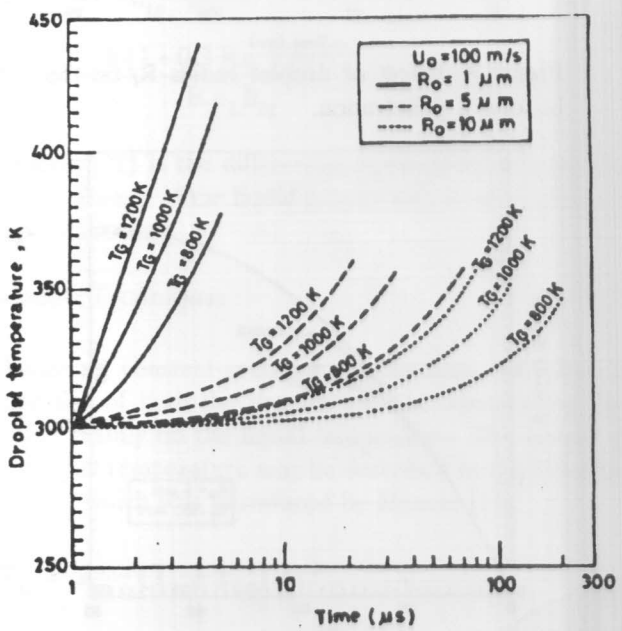

Figure 7. History of droplet temperature.

The Figure shows that the temperature rises faster as the droplet initial radius R_o gets smaller or as the gas temperature T_G is higher. The heat capacity for smaller droplets allows faster rates of temperature rise meanwhile the extremely high gas temperatures accelerate the rate of heat transfer due to the increase in the temperature differential (T_G-T_L). Figure (8) shows that smaller droplets are associated with higher rates of temperature rise dT_L/dt. The rate are higher at T_G = 1200 K than at T_G = 800 K.

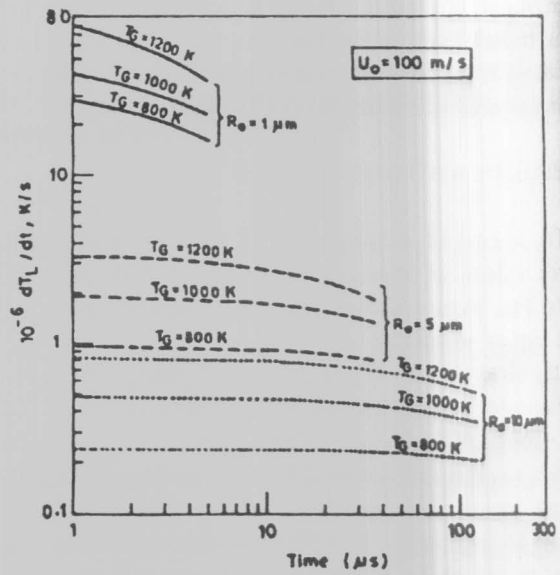

Figure 8. History of rate of temperature change.

The Figure shows that as the evaporation progresses, the value of dT_L/dt decreases because of the slower heat transfer rate due to the decrease in the temperature differential (T_G-T_L). The effect of the droplet velocity U_o on the history of droplet temperature T_L is shown in Figure (9). Five cases ranging between U_o=0 and U_o = 400 m/s are shown for R_o=5μm and T_G = 1000 K.

The Figure shows that increasing the initial velocity of droplet would enhance the heat transfer rate due to the increase in the Reynolds number and the subsequent increase in the Nusselt number (Eq.30). This would result in increasing the droplet temperature at faster rates. The present work was compared to Megahed's [43.] for U_o= and was found to be in agreement with it.

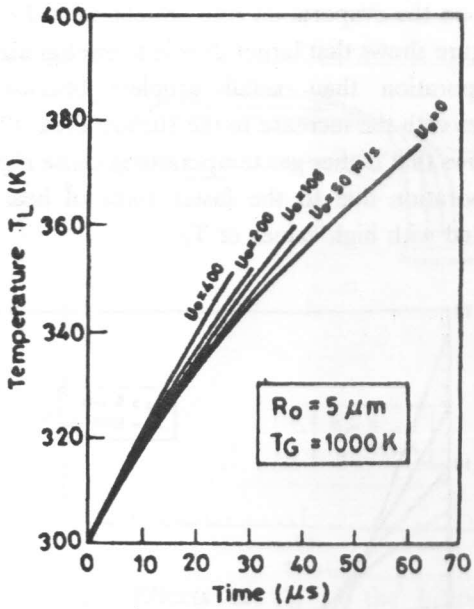

Figure 9. Effect of droplet velocity U_o on the history of droplet temperature T_L.

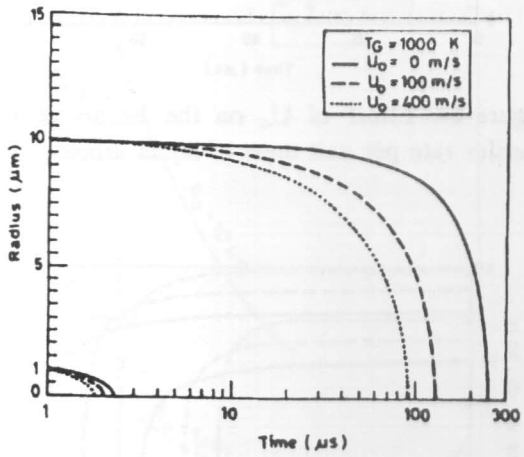

Figure 10. History of droplet radius.

The history of droplet radius is shown in Figure (10) for T_G = 1000 K. Two droplet sizes (R_o = 1, 10 μm) and three droplet velocities (U_o = 0, 100, 400 m/s) are presented. The Figure shows that higher velocities cause higher rates of droplet shrinking due to the higher rates of heat transfer. The results were compared to those by Megahed [43] for U_o = 0, and were found to be in agreement with them. The Figure also shows that small droplets evaporate faster than larger ones.

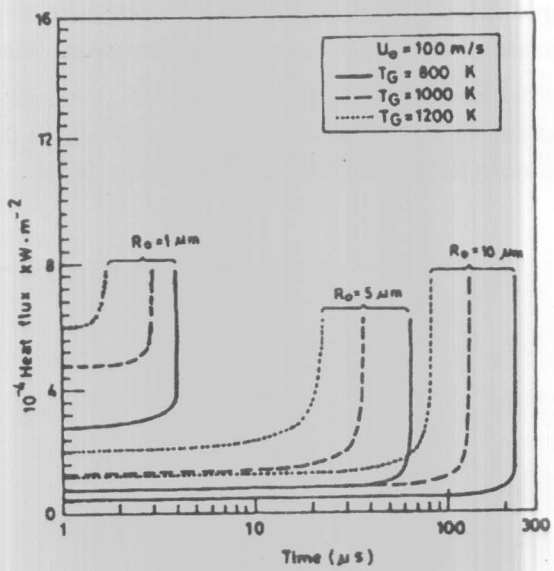

Figure 11. Effects of T_G and R_o on the history of heat flux.

Figure (11) shows the effects of gas temperature T_G and droplet radius R_o on the history of heat flux (kW/m^2) through the droplet surface. The Figure indicates that the heat flux is higher for small droplets than for large ones due to the reduced area for the same rate of heat transfer. The Figure also shows that higher gas temperatures are accompanied by higher values of heat flux due to the increasing temperature differential (T_G-T_L) and the resulting increase in heat transfer rate. The shooting trend of the heat flux is because of the diminishing area of the droplet surface near the end of the evaporation process. Figure (12) shows that higher velocities U_o are accompanied by a higher heat fluxes due to the enhancement of the heat transfer rate.

Figure (13) shows that small droplets have higher rates of heat transfer than larger droplets because the heat transfer coefficient $\bar{h}$ is inversely proportional to the droplet radius (Eq.30). The Figure also shows that higher gas temperatures T_G are associated with higher rates of heat transfer because of the increase in the temperature differential (T_G-T_L). Moreover, Figure (13) shows a gradual decline in the rate of heat transfer as the time of evaporation is elapsed due to the increase in the droplet temperature T_L and the subsequent decrease in (T_G-T_L). Figure (4) shows that the initial heat transfer rate is the highest for U_o = 400 m/s and the lowest for stationary or

suspended droplets (U_o=0) due to the effect of the increasing Reynolds number on increasing the heat transfer coefficient $\bar{h}$. However, as the evaporation rate goes on, the rate of heat transfer for high-velocity droplets decreases faster than that for low-velocity droplets.

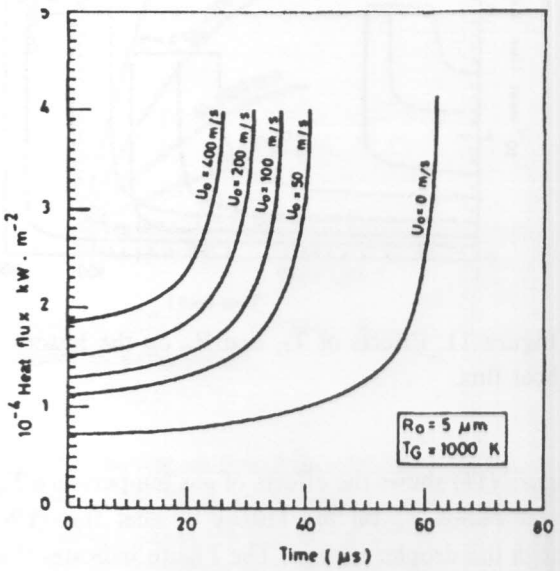

Figure 12. Effect of U_o on the history of heat flux.

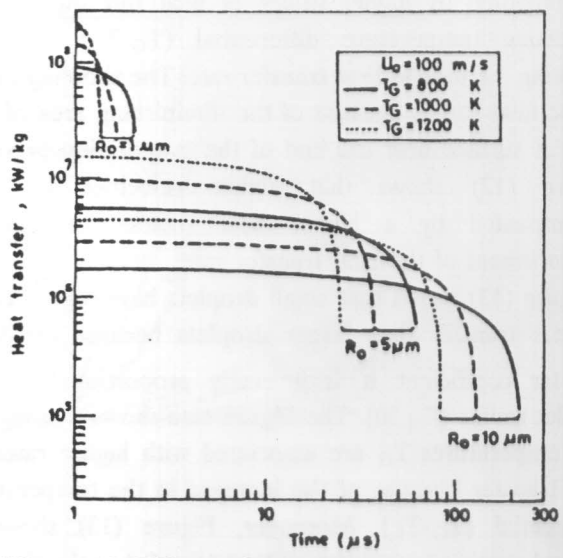

Figure 13. Effects of T_G and R_o on the history of heat transfer rate per unit mass of liquid droplet.

The effects of the gas temperature T_G and the droplet size R_o on the evaporation rate are shown in Figure (15). The Figure shows that larger droplets develop higher rates of evaporation than small droplets because dM/dt increases with the increase in the surface area. The Figure also shows that higher gas temperatures cause higher rates of evaporation due to the faster rates of heat transfer associated with high values of T_G.

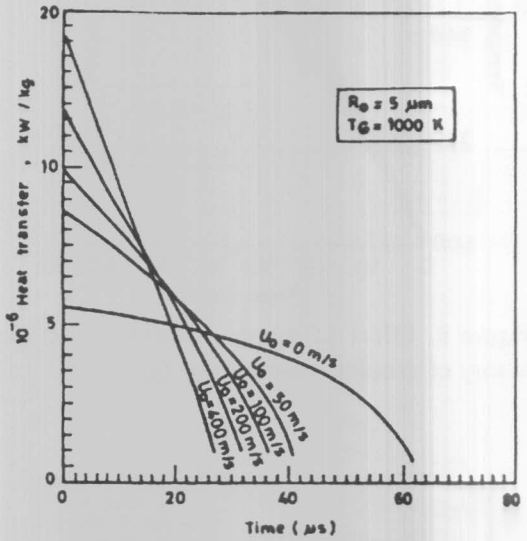

Figure 14. Effect of U_o on the history of heat transfer rate per unit mass of liquid droplet.

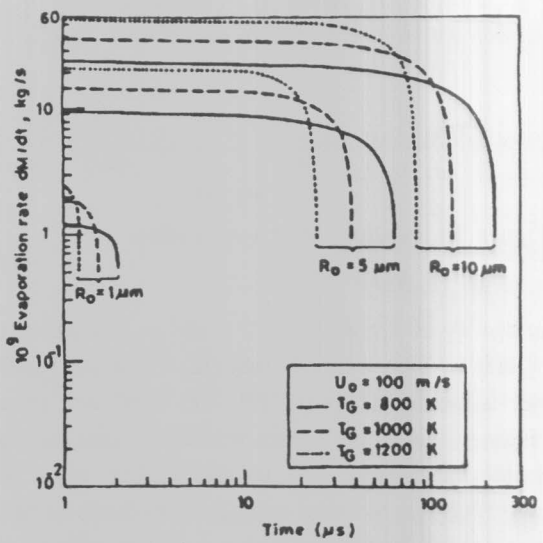

Figure 15. Effects of T_G and R_o on the history of evaporation rate.

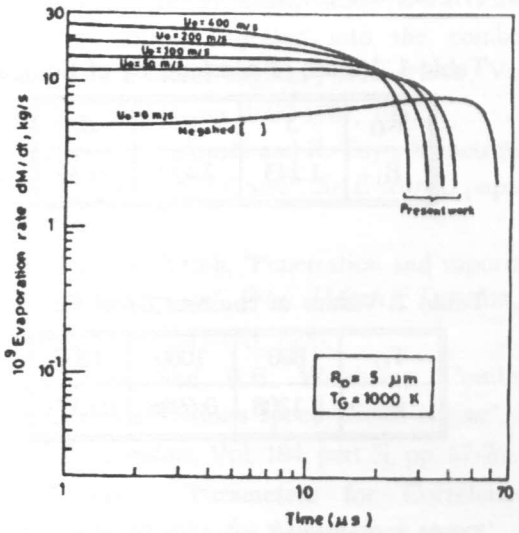

Figure 16. Effects of U_o on the history of evaporation rate.

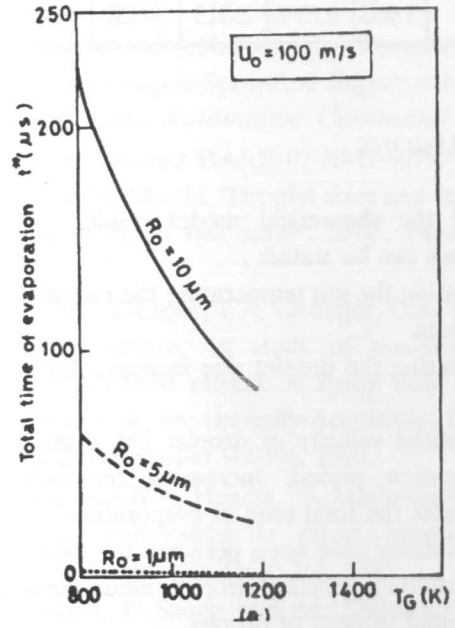

Figure 17. Evaporation time vs. gas temperature T_G.

Figure (16) shows that the increase in the initial velocity U_o of the droplet causes and increase in the evaporation rate due to the associated increase in the mass transfer coefficient.

The evaporation time t^* for various droplet sizes is plotted vs. the gas temperature T_G in Figure (17). The results are shown for the same initial velocity $U_o = 100$ m/s. The Figure shows that the evaporation period is shortened at higher gas temperatures and for smaller droplet sizes.

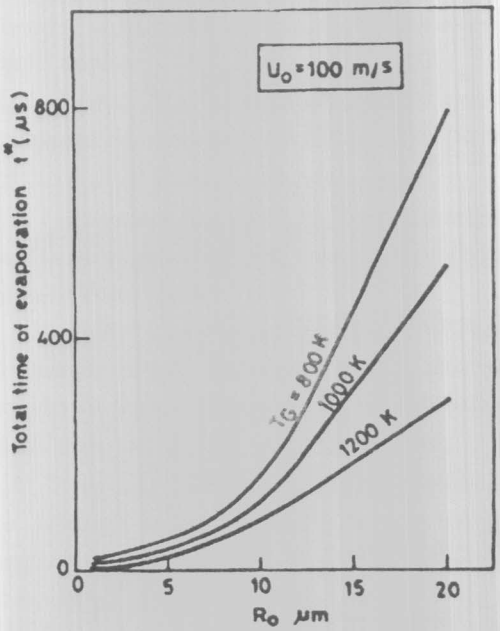

Figure 18. Evaporation time vs. droplet radius R_o.

Figure (18) shows the evaporation time of fuel droplets vs. the initial droplet radius for T_G =800, 1000, and 1200 K. The results are shown for the same initial velocity $U_o = 100$ m/s. The Figure shows a parabolic relationship in which the evaporation time increases with the droplet radius. Finally, the evaporation time is plotted vs. the initial droplet velocity in Figure (19.a) where t^* decreases with the increase in U_o. The velocity effect is more influential for large droplets than for smaller ones, and at low gas temperatures than at higher temperatures. The Figure also shows that most of the velocity effect is obtained within the range of $0 < U_o < 100$ m/s. Any further increase in the initial velocity U_o would slightly reduce the evaporation time. The logarithmic plot of this relationship is shown in Figure (19.b).

According to the present results and the logarithmic plots of Figures (17), (18), and (19), the following

relationships have been deduced:

$$\ln t^* = (2.385\pm0.045)(1000/T_G) + B_1 \quad (35)$$

provided that

$5 \le R_o \le 20\,\mu m,\ 800 \le T_G \le 1200\,K,\ U_o = 100\,m/s$

$$\ln t^* = (1.755\pm0.105)\ln R_o + B_2 \quad (36)$$

provided that

$800 \le T_G \le 1200\,K,\ 5 \le R_o \le 20\,\mu m,\ U_o = 100\,m/s$

$$\ln t^* = (0.025\pm0.005)(1000/U_o) + B_3 \quad (37)$$

provided that

$5 \le R_o \le 10\,\mu m,\ 800 \le T_G \le 1200\,K,$

$50 \le U_o \le 400\,m/s$

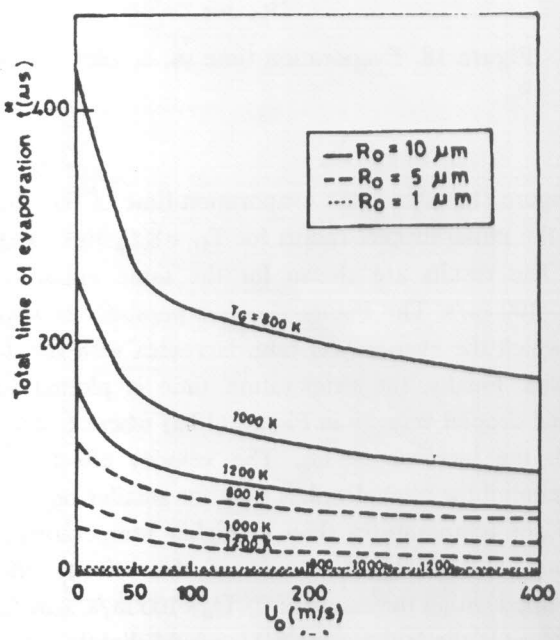

Figure 19. Evaporation time vs. droplet velocity U_o.

The values of the constants B_1, B_2, and B_3 are given in tables (1), (2), and (3), respectively.

Table 1. Values of constant, B_1 of Eq. (35).

R_O	5	10	20
B_1	1.243	2.437	3.639

Table 2. Values of constant B_2 of Eq. (36).

T_G	800	1000	1200
B_2	1.1208	0.6986	0.6373

Table 3. Values of constant B_3 of eq. (37).

R_O, μm	5			10		
T_G, K	800	1000	1200	800	1000	1200
B_3	3.905	3.311	2.813	5.020	4.542	4.095

CONCLUSIONS

Out of the theoretical model results, the following conclusions can be stated:

1. Increasing the gas temperature the rate of evaporation increases.
2. Decreasing the droplet size increases the evaporation rate.
3. The initial velocity of droplet has a great effect on evaporation period. Increasing the initial velocity decreases the total time of evaporation.
4. Correlations have been obtained for the total time of evaporation in terms of droplet radius, gas temperature and initial velocity of droplet.

REFERENCES

[1] P.H. Schweitzer, "Penetration of oil sprays", *The Pennsylvania State University Bulletin*, No. 46, 1937.

[2] A.S. Lyshevskiy, "The Coefficient of free turbulence in a Jet of Atomized Liquid fuel", *NASA*, TT-F 351

1956.

[3] M. Ogasawara and H. Sami, "Study on the behaviour of a fuel droplet injected into the combustion chamber of a diesel engines", *SAE trans.*, Vol. 78, paper No. 670468, pp. 1690-1707, 1967.

[4] M.V. Parks, C. Polonski and R. Toye, "Penetration of Diesel fuel sprays in Gases", *SAE trans.*, paper No. 660747, 1966.

[5] R. Burt and K. Troth, "Penetration and vaporization of Diesel fuel sprays", *Proc. IMechE London,* Vol. 184, part 3j, pp. 147-170, 1970.

[6] D.H. Taylor and B.E. Walsham, "Combustion processes in a Medium speed Diesel engine", *Proc. IMechE, London,* Vol. 184, part 3j, pp. 67-76, 1970.

[7] T.J. Williams, "Parameters for Correlation of Penetration Results for Diesel fuel sprays", *Proc. IMechE.,* London, Vol. 187, pp. 771-774, 1973.

[8] H. Hiroyasu, T. Kadota and M. Arai, "Supplementary Comments: Fuel Spray", Characterization in Diesel Engine in GM.R.C., Michigan, 1978.

[9] N.A. Henein and A.N. Fragoulis, "Penetration Mean Diameter for Liquid Sprays", *A Report submitted to the U.S. Tank Automative Command, Warren,* Michigan, Contract DAAE 07-80-G-9079, 1984.

[10] J. Koo and J. Martin, "Droplet sizes and velocities in a transient diesel fuel spray", *SAE*, Paper 900397, 1990.

[11] M.I. Arold, C. Espey, T.A. Litzinger, D.A. Santavicca and R.J. Santoro, "A study of non-swirling and swirling and their effects on spray flow fields and combustion in an optically-Accessible DI Diesel Engine", *SAE*, Paper 900396, 1990.

[12] T. Singh and N.A. Henein, "A Mathematical model for spray penetration in direct injection diesel engines", *ASME,* (85-DGP-16), 1985.

[13] T. Kiichiro, J. Senda and M. Shikuya, "Transient characteristics of fuel atomization and droplet size distribution in diesel fuel spray", *SAE* (830449), 1983.

[14] M.M. El-Kotb, "Spray-Gas Stream Interaction in Diesel Engines", *The 4th Intl. Conference on Liquid Automization, and Spray Systems, the Fuel Society of Japan*, Sendai, Japan, 22-24 August 1988.

[15] S.K. Aggarwal, A.Y. Tong and W.A. Sirignano, "A comparison of vaporization model in spray calculations" *AIAA* J. vol. 22, (10), pp 1448-1457, 1984.

[16] G.A.E. Godsave, "Studies of the combustion of Drops in a fuel spray-The burning of single drops of fuel" *Fourth symp. (Int) on combustion* pp. 818-830 1952.

[17] N.A. Henein, "A Mathematical Model for the Mass Transfer and Combustible Mixture Formation around Fuel Droplets", *SAE* Paper 710221 1971.

[18] G.M. Faeth, "The kinetics of droplet ignition in a Quiescent Air environment *Ph.D. Dissertation The Pennsylvania State University,* 1964.

[19] P.A. Lakshminarayan and J.C. Dent, "Interferometric studies of vapourising and combustion sprays" *SAE* Paper 830244, 1983.

[20] S. Prakash and W.A. Sirignano, "Theory of Convective droplet vaporization with unsteady heat transfer in the circulating liquid phase", *Int. J. Heat mass transfer*, 23, (3), pp. 253-268 1980.

[21] A.Y. Tong and W.A. Sirignano, "Analytical solution for diffusion in the core of a droplet with internal circulation" *AIchE Symp. Series, heat transfer*, Milwaukee, pp. 400-407, 1981.

[22] J.H. Van Gerpen, C.J. Huang and G.L. Borman, "The effect of Swirl and injection parameters on diesel combustion and heat transfer", *SAE* Paper 850265, 1985.

[23] M.M. Megahed, M.N. Saeed, M.M. Sorour and M.B. Madi, "Unsteady vaporization of stationary dodecane and Alcohol droplets suspended in a hot non-reactive environment", *Int. J. heat Mass transfer,* 1989.

[24] E.F. Joachim, "Oil spray investigations of the N.A.C.A.", *ASME Trans.*, 1927.

[25] F. Pischinger, "Verfahren zur untersuchung von diesel-Einspritzs-rahlen", *Maschbau Warmew,* 10, 1955.

[26] C.K. Westbrook, "Three dimensional Numerical modelling of liquid fuel sprays", *The sixteenth symp. on combustion,* 1977.

[27] A. Cliffe, "A finite difference calculation of spray combustion in turbulent swirling flow", *Int. conference on numerical methods,* SwanSea, U.K. 1977.

[28] F.V. Bracco, "Theoretical Analysis of stratified

two-phase wankel engine combustion", *Combustion science and Tech. 8 Nos 1 and 2* pp. 69-84, 1973.

[29] C.T. Crowe, "A computational model for the gas-droplet flow field in the vicinity of an automizer" *Proc. of the llth JANAF Symp.*, paper 76-23, 1974, ICLASS, 1978.

[30] R.C. Reid, J.M. Prausnitz and T.K. Sherwood, "*The properties of Gases and Liquids*", 3rd Edition, McGraw-Hill, N.Y., 1977.

[31] K.M. WAtson, *Ind. Eng. Chem.*, Vol. 35, p. 398, 1943.

[32] D.S. Viswanath and N.R. Kuloor, *Can. J. Chem. Eng.*, Vol. 45, p. 29, 1967.

[33] T.Z. Lyman and R.P. Danner, *AICHEJ.*, Vol. 22, p. 759, 1976.

[34] R.D. Gunn and T. Yamada, *AICHEJ.*, Vol. 17, p. 1341, 1971.

[35] L.W. Flynn and G. Thodos, *J.* Chem. Eng. Data, Vol. 6, p. 457, 1961.

[36] P. Yoon and G. Thodos, *AICHEJ*, Vol-16, p. 300, 1970.

[37] W.F. Calus and M.T. Tyn, *J. Chem. Eng. Data,* Vol. 18, p. 377, 1973.

[38] S. Chapman and T.G. Cowling, *The Mathematical Theory of Nonuniform Gases*, Cambridge University press, N.Y., 1939.

[39] W.M. Rohsenow and J.P. Hartnett, *Handbook of Heat Transfer*, McGraw-Hill, N.Y., 1973.

[40] D. Roy and G. Thodos, *Ind. Eng. Chem. Fundam.*, Vol. 7, p. 529, 1918.

[41] B. Ewing and W. Galen, *Instrumental Methods of Chemical Analysis,* Fourth Edition, McGraw-Hill, Kogakusha, 1975.

[42] W.E. Ranz and W.R. Marshall, "Evaporation from drops", *Chem. Engg. Prog.* 48 (3), pp. 141-148, 1952.

[43] M.M. Megahed, "Multicomponent Droplet Vaporization and its Application to Alcohol-Dodecane Mixtures", *M.Sc. Thesis*, Alexandria University, 1988.